Hydrogels for Flexible and Compressible Free Standing Cellulose Supercapacitors

Maricruz G. Saborío,[1,2] Petra Svelic,[1] Jordi Casanovas,[3] Guillem Ruano,[1,2] Maria M. Pérez-Madrigal,[1,2] Lourdes Franco,[1,2] Juan Torras,[1,2] Francesc Estrany,[1,2,*] and Carlos Alemán[1,2,4,*]

[1] *Departament d'Enginyeria Química, EEBE, Universitat Politècnica de Catalunya, C/ Eduard Maristany 10-14, Ed. I2, 08019 Barcelona, Spain*

[2] *Barcelona Research Center for Multiscale Science and Engineering, Universitat Politècnica de Catalunya, Eduard Maristany 10-14, 08019 Barcelona, Spain*

[3] *Departament de Química, Escola Politècnica Superior, Universitat de Lleida, c/Jaume II no. 69, Lleida E-25001, Spain*

[4] *Institute for Bioengineering of Catalonia (IBEC), The Barcelona Institute of Science and Technology, Baldiri Reixac 10-12, 08028 Barcelona, Spain*

[*] Corresponding authors: francesc.estrany@upc.edu and carlos.aleman@upc.edu

ABSTRACT

Cellulose-based supercapacitors display important advantages in comparison with devices fabricated with other materials, regarding environmental friendliness, flexibility, cost and versatility. Recent progress in the field has been mainly focused on the utilization of cellulose fibres as: structural mechanical reinforcement of electrodes; precursors of electrically active carbon-based materials; or primary electrolytes that act as reservoirs of secondary electrolytes. In this work, a flexible, lightweight, robust, portable and manageable all-carboxymethyl cellulose symmetric supercapacitor has been obtained by assembling two electrodes based on carboxymethyl cellulose hydrogels to a solid electrolytic medium formulated with the same material. Hydrogels, which were made by cross-linking carboxymethyl cellulose paste with citric acid in water, rendered not only effective solid electrolytic media by simply loading NaCl but also electroactive electrodes. For the latter, conducting polymer microparticles, which were loaded into the hydrogel network during the physical cross-linking step, were appropriately connected through the *in situ* anodic polymerization of a similar conducting polymer in aqueous medium, thus creating conduction paths. The performance of the assembled supercapacitors has been proved by cyclic voltammetry, galvanostatic charge-discharge and electrochemical impedance spectroscopy. This design opens a new window for the green and mass production of flexible cellulose-based supercapacitors.

INTRODUCTION

Since General Electric patented them in 1957, supercapacitors have attracted a great deal of attention because of their features: high power density and rate capability, fast energy uptake and delivery, long cycle life, simple principles, adequate thermal stability, and low maintenance cost [1]. Charge is stored in a supercapacitor device through a double-layer electrostatic mechanism (*i.e.* adsorption and desorption of charged ions from an electrolyte onto highly porous electrodes) and/or a faradic redox process (*i.e.* pseudocapacitance, which is based on fast and reversible surface redox reactions). Conducting polymers (CPs) are appropriate electrode materials for pseudocapacitors, also named *electrochemical supercapacitors* (ESCs) [2], since they have higher conductivity and capacitance than some carbon electrode materials (*e.g.* activated carbon, carbon nanotubes and carbon aerogels) even though their cycling stability is lower.

In the last decade, significant efforts have been devoted to fabricate flexible energy storage devices, including supercapacitors [3-11]. Compared with conventional devices, flexible supercapacitors are portable, bendable and even wearable or implantable. These optimized and superior characteristics will facilitate the development of electronic devices with different functionalities, such as roll-up displays, smart mobile devices, and implantable biosensors, among others. Both carbon materials and polymers provide important advantages for the manufacturing of supercapacitors since, in addition to flexibility, they render lightweight products. However, most of them derive from petroleum and, therefore, the environmental concerns arouse during their preparation and complicated manufacturing, thus largely limiting their applications in supercapacitor devices. Because of these limitations, research on flexible supercapacitors has been focused on materials that can be easily obtained from natural

sources [12]. Within this context, the utilization of green biopolymers extracted from biomass or their derivatives to produce porous organic materials has been considered critical to reach sustainable development and protect the environmental [13]. The most abundant and sustainable biopolymer is cellulose since it is an important structural component of the primary cell wall of green plants.

Cellulose fibres exhibit high aspect ratios, high surface area, high porosity, excellent mechanical properties, excellent flexibility, and the ability to bind to other conductive materials, enabling extensive application in flexible energy-storage devices [14,15]. The very extensive literature about electrically active cellulose-based devices for energy applications, which has been critically analysed in some seminal reviews [16-21], evidences two important features. First, the role played by cellulose in the fabricated flexible supercapacitors is usually restricted to one of the following three: 1) structural mechanical reinforcement that confers flexibility and strength to the electrodes, which contain other electrically active materials; 2) precursor (raw material) of other electrically active carbon-based materials obtained by pyrolytic processes; or 3) primary electrolyte that connects the two electrodes by acting as a reservoir of secondary electrolytes (*i.e.* small ions) [16-21]. In spite of this versatility, flexible all-cellulose supercapacitors, which were considered a chimera a few decades ago, are still to come. Second, cellulose-containing supercapacitors are mainly based on fibres format, while hydrogels are used to a lesser extent. More specifically, cellulose hydrogels have been exclusively used as electrolyte reservoirs to favour ion movement towards the supercapacitor double layer [22-24]. Therefore, the potential application of cellulose hydrogels as electrodes in flexible supercapactitors awaits development.

In this work, we report a simple procedure to fabricate compact and deformable all-carboxymethyl cellulose solid *organic electrochemical supercapacitors* (OESCs) using

carboxymethyl cellulose sodium salt (NaCMC) as the main component of the two electrodes (*i.e.* the anode and the cathode) and the solid electrolyte. Moreover, both NaCMC-based OESC elements have been prepared exploiting the advantages of the hydrogel format. More specifically, the self-supported and flexible electrodes have been prepared by embedding CP- and alumina-based (Al_2O_3) particles in NaCMC hydrogels and, then, performing an *in situ* anodic polymerization in aqueous conditions, whereas the solid electrolyte consists of a NaCMC hydrogel loaded with NaCl as supporting electrolytic salt. Hydrogels for both the electrodes and the solid electrolyte were prepared by directly cross-linking NaCMC chains in a citric acid aqueous solution at room temperature and atmospheric pressure. This approach has allowed us to enhance some of the main principles of green chemistry: *i*) avoid, or reduce as much as possible, the consumption of organic solvent; *ii*) use low-energy consumption processes avoiding high temperature and/or pressure; *iii*) avoid chemical derivatives that use additional reagents and generate waste; and *iv*) prioritize the utilization of materials extracted from renewable natural sources).

RESULTS AND DISCUSSION

Preparation and characterization of flexible NaCMC-based electrodes

The first step for preparing flexible electrodes involved the loading of microparticles into the NaCMC biohydrogel of 20% w/w poly(3,4-ethylenedioxythiophene) (PEDOT) microparticles (MPs) dispersed in basic aqueous solution (0.5 M $NaHCO_3$) and 2% w/w Al_2O_3 (*i.e.* the wt. % of both PEDOT and Al_2O_3 MPs was referred to the weight of NaCMC). PEDOT is one of the most used CPs for energy storage devices because of its excellent electrochemical and electrical properties [25-27], its combination with cellulose being particularly attractive because of the well-known non-toxic and

biocompatible behaviour of this CP [28,29]. For the synthesis of PEDOT MPs, CP films were prepared by chronoamperometry applying a constant potential of 1.40 V and adjusting the polymerization charge to 120 mC [30,31]. The resulting films were removed from the steel electrodes and, subsequently, processed into MPs that display a diameter of 3.0±1.2 µm by mechanical stirring (Figure 1a). On the other hand, the homogenization and size reduction of Al_2O_3 MPs, which were loaded into the biohydrogel to enhance the electrochemical properties of PEDOT [32], was essential to ensure a good dispersion within the NaCMC matrix. After stirring, Al_2O_3 MPs with diameters ranging from ~1 to ~10 μm were obtained (Figure 1b).

Both PEDOT and Al_2O_3 MPs were introduced in the cellulose paste, which consisted in an extremely high viscous aqueous solution obtained by pouring 10 % wt. NaCMC in water and mixing (Electronic Supplementary Information). The PEDOT- and Al_2O_3-loaded NaCMC paste was transformed into a self-standing PEDOT/Al_2O_3/NaCMC hydrogel by cross-linking the cellulose chains with citric acid. For this purpose, the paste was immersed into 8 M citric acid solution for 24 hours at room temperature under moderate shaking (80 rpm) (Figure 1c). In this acidification step, Na^+ of NaCMC polymer backbones were gradually replaced by H^+ and the hydrogel was constructed by physical cross-linking along with the formation of hydrogen bonds between the neighboring polymer chains [33].

After this, the performance of the flexible PEDOT/Al_2O_3/NaCMC electrodes was enhanced by incorporating poly(hydroxymethyl-3,4-ethylenedioxythiophene) (PHMeDOT) inside the hydrogel through *in situ* anodic polymerization. To that end, the hydrogel was attached to a steel sheet and immersed in a 50 mM hydroxymethyl-3,4-ethylenedioxythiophene monomer (HMeDOT) aqueous solution with $LiClO_4$, which was kept under stirring during 1.5 hours to ensure the penetration of the monomer into

the hydrogel matrix. This step was crucial to ensure the access of the HMeDOT monomer to the PEDOT MPs, which act as polymerization nuclei. The anodic polymerization was conducted at pH 8 under a constant potential of 1.10 V for 2 hours. The latter time was optimized to achieve the connection among PEDOT MPs through the polymerized PHMeDOT (*i.e.* the percolation of the CPs), as shown below. Although the electrochemical properties of PHMeDOT and PEDOT are very similar, the solubility of HMeDOT in water, which is the solvent used in the reaction medium, is higher than that of EDOT [30-32,34]. This process is illustrated in Figure 1d, while details are provided in the Electronic Supplementary Information. Hereafter, the electrodes obtained after the *in situ* polymerization of HMeDOT are denoted [PEDOT/Al$_2$O$_3$/NaCMC]PHMeDOT.

Low and high resolution SEM micrographs of PEDOT/Al$_2$O$_3$/NaCMC and [PEDOT/Al$_2$O$_3$/NaCMC]PHMeDOT are displayed in Figures 2a and 2b, respectively. As it can be seen, the porous structure of PEDOT/Al$_2$O$_3$/NaCMC remains unaltered after the *in situ* polymerization of the HMeDOT monomer, CP particles becoming more accessible after this process. Thus, PHMeDOT polymerizes coating the PEDOT MPs, as is evidenced in Figure 2c, but also forming thin sticks that connect the CP MPs through effective conduction paths. It is worth noting that these MP-connecting sticks, which are displayed in Figure 2b (inset) and Figure 2d, are not observed in PEDOT/Al$_2$O$_3$/NaCMC. Moreover, this unique structure is present at the surface of the [PEDOT/Al$_2$O$_3$/NaCMC]PHMeDOT electrode, as well as in the inner region (Figure 2e).

The FTIR spectra of NaCMC, PEDOT/Al$_2$O$_3$/NaCMC and [PEDOT/Al$_2$O$_3$/NaCMC]PHMeDOT lyophilized hydrogels are compared in Figure 3a. The broad absorption band in the region 3000-3700 cm^{-1}, which appears in all three

spectra, has been attributed to the stretching of the free and bonded hydroxyl groups of NaCMC and PHMeDOT. The peak at around 2895 cm^{-1} is assigned to the aliphatic saturated C–H stretching vibration of NaCMC matrix. The peak at 1720 cm^{-1} is attributed to the carbonyl band of –COOH, coming from the substitution of Na$^+$ to H$^+$ in the polymer chains, indicating that acidification with citric acid favors physical cross-links in cellulose [33]. The very strong bands at 1058 and 1110 cm^{-1} are attributed to the C–O–C and C–O pyranose ring skeletal vibrations, respectively. The presence of PEDOT MPs is typically disclosed by the appearance of the vibrations associated to the dioxane ring, even though in this case such bands overlap with those of the pyranose ring. The FTIR spectrum of PEDOT/Al$_2$O$_3$/NaCMC contains a peak at 1520 cm^{-1} that is due to the C=C stretching of the thiophene ring. Anodic polymerization of PHMeDOT results in the enhancement of the peaks at 1318 and 1419 cm^{-1}, which correspond to other skeletal vibrations of the aromatic thiophene rings and are very weak for PEDOT/Al$_2$O$_3$/NaCMC. Moreover, the strong peaks at 1595 cm^{-1} in the FTIR spectrum of [PEDOT/Al$_2$O$_3$/NaCMC]PHMeDOT has been associated to enhanced oxidation processes.

Raman spectra of NaCMC, PEDOT/Al$_2$O$_3$/NaCMC and [PEDOT/Al$_2$O$_3$/NaCMC]PHMeDOT samples corroborated the homogeneous integration of the CPs into the NaCMC matrix. Thus, the spectra reported in Figure 3b exhibit the characteristics peaks of PEDOT and PHMeDOT: 985 cm^{-1} (vibration mode of the thiophene C–S bond), 1099 cm^{-1} (stretching of the ethylendioxy group), 1255 cm^{-1} (C–C inter-ring stretching), 1367 cm^{-1} (C–C stretching), 1423 cm^{-1} (C=C symmetrical stretching) and 1489 cm^{-1} (C=C asymmetrical stretching).

Theoretical Density Functional Theory (DFT) calculations on model complexes were conducted to examine the favourable interaction between the NaCMC and the CPs.

More specifically, calculations were performed using the M06L functional [35] combined with the 6-31G(d,p) basis set. NaCMC was modelled considering three model compounds (denoted CMCn with $n=$ 1, 2 or 3 in Figure 3c) with two glucopyranose monomers, which differ in the position of the carboxymethyl (CH$_2$COOH) substituent. Besides, PEDOT was simplified to a model oligomer containing 2 repeat units (hereafter 2EDOT). For complexes in which 2EDOT was in the reduced states (charge= 0), the carboxymethyl substitutent was protonated (CH$_2$COOH), whereas the latter was ionized (CH$_2$COO$^-$) when 2EDOT was in the oxidized state (charge= +1) state. CMCn···2EDOT and CMCn···2EDOT^{+1} model complexes were subjected to complete geometry optimizations. The binding energy (BE), which is defined by subtracting the energy of individual components from the energy of the complex, was evaluated eliminating the basis set superposition error [36]. In order to evaluate the strength of electrostatic interactions in CMCn···2EDOT^{+1} complexes, the BE of CMCn···Na$^+$ and ClO$_4^-$···2EDOT^{+1} model complexes was also determined using DFT calculations at the same theoretical level. Although for all the studied complexes different starting structures were constructed by varying the relative position between the two interacting species, only the most stable structure of each optimized complex has been considered for discussion.

Figures 3d and 3e compare the BEs of neutral (*i.e.* CMCn···2EDOT) and charged complexes (*i.e.* CMCn···2EDOT^{+1}, CMCn···Na$^+$ and ClO$_4^-$···2EDOT^{+1}), respectively. Attractive BE values were obtained in all cases, indicating that NaCMC and PEDOT repeat units interact favourably. Moreover, the BEs of CMCn···2EDOT complexes are practically independent of the position of the carboxymethyl substituent, while the BEs of CMCn···2EDOT^{+1} complexes exhibit a variability of ~4%. Besides, the BEs of CMCn···2EDOT complexes, which are mainly stabilized through specific hydrogen

9

bonds, represents ~20% of the BE values obtained for CMCn···2EDOT^{+1} in which non-specific electrostatic interactions play a key role.

The affinity between PEDOT and NaCMC is explained by comparing the BE values obtained for CMCn···2EDOT^{+1}, which range from -87.2 to -90.8 kcal/mol, with those of CMCn···Na$^+$ and ClO$_4^-$···2EDOT^{+1}. Thus, the CMCn···Na$^+$ complexes, with BE values comprised between -130.3 and -143.0 kcal/mol, are electrostatically stabilized by strong intermolecular interactions. In contrast, the weakest interaction corresponds to the ClO$_4^-$···2EDOT^{+1} complex, with BE= -76.7 kcal/mol, suggesting that the perchlorate dopant ions could be replaced by the carboxylate groups of NaCMC if Na$^+$ counter-ions leave with them. However, the strength of the electrostatic interaction in NaCMC regulates the latter process and drastically limits the replacement degree that, despite this restriction, is high enough to immobilize PEDOT MPs. Overall theoretical calculations are consistent with experimental observations in which PEDOT MPs integrate into the NaCMC matrix but retaining their own identity.

Preparation and characterization of NaCMC hydrogel as solid electrolyte

Sustainable NaCMC hydrogels containing a salt as supporting electrolyte were prepared as solid state electrolyte for compact cellulose-based OESCs. This was achieved using the procedure described above to produce PEDOT/Al$_2$O$_3$/NaCMC flexible electrodes but replacing the PEDOT and Al$_2$O$_3$ particles by 0.5 M NaCl as supporting electrolytic salt. After the gelation of the NaCMC paste with citric acid, the excess of acid was eliminated by washing, causing the partial loss of the supporting electrolytic salt. In order to recover such salt, washed hydrogels were submitted to a reabsorption process by immersion in a 0.5 M NaCl solution for 24 hours. Hereafter, the

hydrogel obtained after the post-washing treatment to recover supporting electrolytic salt is denoted NaCMC/NaCl.

Figure 4a compares the swelling ability, as determined from the swelling ratio (SR), of the NaCMC/NaCl and [PEDOT/Al$_2$O$_3$/NaCMC]PHMeDOT in 0.1 M NaHCO$_3$. Although the SR of the latter is significantly lower than that of the former, which indicates that the CPs restricts the moisture content, both values are relatively low. Thus, after 24 h, the SR was 1064% and 623% for NaCMC/NaCl and [PEDOT/Al$_2$O$_3$/NaCMC]PHMeDOT, respectively. These values are much smaller than that reported for NaCMC hydrogels prepared using a 1.5 M citric acid (SR= 2205%) [24], reflecting the remarkable influence of the citric acid concentration in the cross-linking density. Thus, the water-content decreases considerably when the citric acid concentration increases from 1.5 M to 8 M, which is indicative of an increment in the cross-linking. This pronounced effect, which is evidenced in Figure 4a by the photographs of NaCMC/NaCl and [PEDOT/Al$_2$O$_3$/NaCMC]PHMeDOT hydrogels (whitish and dark blue, respectively), is expected to favour the dimensional stability of cellulose-based solid OESC (see below).

SEM micrographs of NaCMC/NaCl with different magnifications are displayed in Figure 4b. As it can be seen, the hydrogel presents an open structure with abundant pores and cavities, which will be necessary to maximize the pseudocapacitance of [PEDOT/Al$_2$O$_3$/NaCMC]PHMeDOT electrodes in the OESC device. Hence, such opened structure will facilitate the ion migration at the electrode-solid electrolyte interface during charge-discharge processes. Moreover, pores, which present an average size of 78±36 μm, are interconnected due to the high concentration of citric acid used in the cross-linking process.

Thermogravimetric analyses (TGAs) of NaCMC/NaCl, PEDOT/Al_2O_3/NaCMC and [PEDOT/Al_2O_3/NaCMC]PHMeDOT hydrogels are displayed in Figure 4c. The mass loss of 12% below 100 ºC has been attributed to the removal of absorbed water. A very pronounced degradation step is displayed by NaCMC, the maximum temperature of differential thermal gravimetric analysis (DTGA) curve being located at 221 ºC. The char weight rendered at 590 ºC was of 18%, which was attributed to the supporting electrolytic salt. The TGA profile recorded for the PEDOT/Al_2O_3/NaCMC hydrogel, which shows two well-defined degradation steps, indicates that the incorporation of PEDOT and Al_2O_3 causes important changes. The first degradation step, which has been associated with the NaCMC matrix, points that the thermal stability of cellulose matrix is significantly enhanced by PEDOT and Al_2O_3. More specifically, the maximum of the corresponding DTGA curve increases from 221 ºC for NaCMC/NaCl to 275 ºC, which represents an increment of 54 ºC. The second degradation step, which corresponds to the maximum at 362 ºC in the DTGA curve, has been attributed to the degradation of PEDOT. It is worth noting that the latter value is similar to that previously reported for pristine PEDOT and PEDOT/Al_2O_3 [32]. In this case, the charge yield at 590 ºC corresponds to 34%, the increment with respect to the NaCMC/NaCl being due to both the incorporated Al_2O_3 and the dopant agent of the CP (*i.e.* perchlorate anions).

Finally, the TGA and DTGA curves obtained for [PEDOT/Al_2O_3/NaCMC]PHMeDOT show three degradation steps located at 252, 280 and 348 ºC (Figure 4c). The latter value corresponds to the degradation of the PEDOT nuclei coated with electropolymerized PHMeDOT, while the two former maxima have been associated to different regions of the NaCMC matrix. Thus, the splitting of the NaCMC degradation peak has been attributed the presence of regions without

PHMeDOT and regions in which the CP integrates into the cellulose matrix forming strong NaCMC···PHMeDOT interactions. Furthermore, the application of a constant potential during the *in situ* anodic polymerization of the CP may induce the rupture of some chemical bonds in the cellulose matrix and, therefore, the degradation of the NaCMC polymer chains.

Assembly of the cellulose-based OESC

The solid and compact cellulose-based OESC was built by connecting two [PEDOT/Al$_2$O$_3$/NaCMC]PHMeDOT electrodes, which acted as cathode (C) and anode (A), through a NaCMC/NaCl solid electrolytic medium (SE), as is schematically represented in Figure 5a. For this purpose, both [PEDOT/Al$_2$O$_3$/NaCMC]PHMeDOT and NaCMC/NaCl hydrogels were prepared using steel ring templates (Figure 5b) with internal diameter and height of 10 and 3.5 mm, respectively. One and two coupled steel rings were used for the preparation of electrodes and the solid electrolytic medium, respectively, the height of the final prototype being 14 mm (Figure 5c). The assembly of the OESCs was conducting by moulding on a press (Figure 5c). More specifically, the applied pressure was 5 tons for 5 min and, subsequently, 10 tons for another 5 min (Figure 5d).

In addition of the outstanding flexibility of the OESC elements, which is illustrated in Figure 5e for the SE, the whole device exhibited high compressibility (Figure 5f). Other interesting properties of this cellulose-based OESC are small and controllable dimensions, manageability, portability, robustness and lightweight.

Characterization of the cellulose-based OESC prototype

13

Characterization studies were performed by coupling the assembled OESC to external steel electrodes, as is displayed in Figure 6a. Cyclic voltammograms recorded by varying the initial and final potential from –0.5 V to 0.0 V in increments of +0.1 V while the reversal potential was kept fixed at +0.8 V (scan rate: 50 mV/s) are compared in Figure 6b. The specific capacitance (*SC*) was determined using the following expression:

$$SC = \frac{Q}{\Delta V \cdot m} \tag{1}$$

where Q is voltammetric charge determined by integrating the oxidative (anodic charge) or the reductive parts (cathodic charge) of the cyclic voltammogram, ΔV is the potential window (in V), m is the mass of the CP (in g) in the cellulose-based OESC. The area of the voltammogram and the *SC* decreases with increasing initial/final potential. Thus, *SC* was 1.2, 1.1, 1.1, 0.8, 0.8 and 0.6 mF/g when the initial/final potential was –0.5, –0.4, –0.3, –0.2, –0.1 and 0.0 V, respectively. It is worth noting that cyclic voltammetry is considered as a very aggressive electrochemical technique that frequently degrades organic materials during the potential scanning, as has been demonstrated for both CPs [37] and electroactive hydrogels [30] similar to those employed in this work for the fabrication of the OESC. As such damage increases with the potential window, the choice of initial/final potential for further analyses on cellulose-based OESCs was based on the compromise between loss of *SC* and degradation of the material. More specifically, the 1.1 V window defined by –0.3 V as initial and final potential and +0.8 V as reversal potential, was used to conduct additional studies on the stability of the designed OESC. Moreover, the voltammogram curve obtained for the selected potential window approximates more to the rectangular or quasi-rectangular shape ideally desired for supercapacitors (Figure 6b).

Figure 6c compares the cyclic voltammograms recorded in the selected potential window at scan rates of 50 and 100 mV/s. As it was expected, the area of the voltammetric curves increases with the scan rate. In this case, such phenomenon is accompanied by an enhancement of the voltammetric charge at the working electrode, indicating that the capacitive performance of the prepared OESC increases with the scan rate. However, this capacitive behavior experiences a reduction when consecutive oxidation-reduction cycles are applied. Thus, after 200 redox cycles, the cellulose-based OESC experienced a loss of rectangular shape in the cyclic voltammogram (Figure 6c), which also affected the *SC* (Figure 6d). Thus, the *SC* decreased from 1.1 to 0.8 mF/g after 200 redox cycles (Figure 6d), which represents a reduction of 27%.

As mentioned above, CV is a disruptive technique that frequently damages organic materials, like those studied in this work. Accordingly, the cycling stability of the as-prepared cellulose-based OESC devices was re-examined by applying 2500 galvanostatic charge-discharge (GCD) cycles at a current of 0.00165 mA in the two-electrode configuration (Figure 6e). Both the charge and discharge times, which were $t_c= 6.7$ s and $t_d= 5.5$ s, respectively, for the second cycle, decreased with the increasing number of GCD cycles. Thus, these parameters were $t_c= 5.4$ s and $t_d= 4.4$ s after 2500 cycles, which represent a reduction of ~20%. In spite of this, GCD curves do not exhibit important distortions and changes after 2500 cycles. More specifically, the curves associated to the last ten GCD cycles maintain the quasi-symmetrical shape of the curves corresponding to the first ten cycles (Figure 6f). This is because the difference between the t_c and t_d values does not change significantly after such huge amount of cycles (*i.e.* 1.2 s and 1.0 s for the second and last cycle). Besides, the *SC*, as determined from GCD curves, decreases from 0.9 mF/g (2nd cycle) to 0.7 mF/g (2500th cycle), which represents a reduction of 0.2 mF/g only.

The power density (P, mW/kg), which describes the speed at which the energy stored can be delivered, is maintained at practically the same value after 2500 GCD cycles (*i.e.* P= 176 and 181 mW/kg for the 2nd and 2500th cycle, respectively). Similarly, the maximum energy density (E_{max}, mWh/kg), which is the amount of energy stored per unit of mass, remains at E_{max}= 0.14 (2nd cycle) and 0.11 mWh/kg (2500th cycle). Overall, GCD results indicate that devices obtained using NaCMC hydrogels with CPs inside as electrodes and a NaCMC hydrogel as solid electrolytic medium exhibit mechanical stability, good capacitor response and excellent cycling stability.

Finally, we further explored the electrochemical response of our cellulose-based supercapacitor device by electrochemical impedance spectroscopy (EIS). The impedance was determined for the $10 - 10^5$ Hz frequency interval using a through-plane impedance cell [38]. The Nyquist and Bode plots are displayed in Figure 7. The almost straight line observed in the Nyquist plot (Figure 7a) is consistent with the behaviour typically found electrical double-layer porous capacitors [39]. At high frequencies, the plot shows a very soft semicircle, indicating a fast charge transfer through a Faradaic process with negligible charge transfer resistance. This is consistent with the porous structure of the electrode, which favours the permeation of the electrolyte and enhances the ion transfer kinetics [40]. Besides, the shapes of the Bode plots obtained for the cellulose-based OESC are very similar to those reported for ITO [41], which is a typical conducting material. Although the impedance values obtained for OESC in the 1-10^2 Hz frequency range (Figure 7b) are similar to those found for bare ITO, the interfacial impedance provided by the NaCMC and the CPs improve the sensitivity of the measurements in higher frequency range. The linear portion observed in the middle of the Bode-phase plot (Figure 7c) indicates a diffusion limited process at the electrode-electrolyte interface.

The Randles-Ershler EEC model used for fitting the experimental data from EIS measurements provides not only understanding of the response of the fundamental systems with coupled processes (*e.g.* charge transfer, diffusion, electric double layer charging and uncompensated solution resistance) but also quantification of some fundamental interfacial phenomena. The EEC obtained for the cellulose-based OESC, which is schematized in Figure 7d, is in agreement with those usually observed for gel-based electrodes [42]. The solid electrolyte resistance (R_e), which is mainly due to the NaCl used to prepare the NaCMC/NaCl biohydrogel, is 485 Ω, which is consistent with the semiconducting behaviour of the prototype. On the other hand, the value of the charge-transfer resistance (R_{ct}= 40 Ω) is lower than R_e, facilitating the exchange of ions along the double layer. The R_{ct} is in series with a constant phase element (CPE) impedance, which has been expressed as:

$$Z_{CPE} = \frac{1}{Y_0(jw)^n} \tag{2}$$

where Y_0 is the admittance of an ideal capacitance and *n* is an empirical constant ranging from 0 to 1. The CPE represents a capacitor and a resistor for *n*= 1 and *n*= 0, respectively, while it is associated with a diffusion process when *n*= 0.5 and is equivalent to the so-called Warburg element. In this work, the Z_{CPE} with *n*= 0.873 is related to the ionic diffusion through the electrode. Finally, the double layer capacitance element (C_{dl}), with a value of 4.16 µF, reflects the capacitance at the electrode/electrolyte interphase. The quality of the experimental data fitting to EEC was evaluated to estimate the percentage error associated with each circuit element, being comprised between 0.4% and 5.1% in all cases.

CONCLUSIONS

In this study, we report the preparation and characterization of NaCMC-based OESCs as versatile platforms for energy storage device applications. The approaches used to prepare the hydrogel-based electrodes and electrolytic medium exploit abundant environment-friendly materials and cheap chemical processes that are conducted in aqueous media at room temperature, and thus can be up-scaled for industrial applications. Moreover, the in situ polymerization strategy used for manufacturing the electrodes, which can be easily extended to other CPs, allows us to regulate the energy storage capacity by controlling the polymerization time. Hence, such low-cost, lightweight, self-standing, flexible and stable cellulose-based OESCs offer great promise for advanced energy storage applications where the utilization of conventional devices can be restricted because of surrounding factors (*e.g.* demands regarding conformability, safety, cost and environmental friendliness).

ACKNOWLEDGEMENTS

DATA AVILABILITY

The raw/processed data required to reproduce these findings are available upon request to the authors.

APPENDIX A. SUPPLEMENTARY MATERIAL

Synthetic methods and characterization techniques. Supplementary data to this article can be found online at https://

REFERENCES

1. J. Yan, Q. Wang, T. Wei, Z. Fan, Recent advances in design and fabrication of electrochemical supercapacitors with high energy densities, Adv. Energy Mater. 4 (2014) 1300816.

2. A. M. Bryan, L. M. Santino, Y. Lu, S. Acharya, J. M. D'Arcy, Conducting polymers for pseudocapacitive energy storage, *Chem. Mater.* 28 (2016) 5989–5998.

3. L. Hu, Y. Cui, Energy and environmental nanotechnology in conductive paper and textiles, Energy Environ. Sci. 5 (2012) 6423–6435.

4. K. Jost, G. Dion, Y. Gogotsi, Textile energy storage in perspective, J. Mater. Chem. A 2 (2014) 10776–10787.

5. M. F. El-Kady, R. B. Kaner, Scalable fabrication of high-power graphene micro-supercapacitors for flexible and on-chip energy storage, Nat. Commun. 4 (2013) 1475.

6. F. Sharifi, S. Ghobadian, F. R. Cavalcanti, N. Hashemi, Paper-based device for energy applications, Renew. Sustainable Energy Rev. 52 (2015) 1453–1472.

7. Y. Ko, M. Kwon, K. B. Wan, B. Lee, S. W. Lee, J. Cho, Flexible supercapacitor electrodes based on real metal-like cellulose papers, Nat. Commun. 8 (2017) 536.

8. B. G. Hoi, J. Hong, W. H. Hong, P. T. Hammond, H. Park, Facilitated ion transport in all-solid-state flexible supercapacitors, ACS Nano 5 (2011) 7205–7213.

9. Y. Li, K. Sheng, W. Yuan, G. A. Shi, A high-Performance flexible fibre-shaped electrochemical capacitor based on electrochemically reduced graphene oxide, Chem. Commun. 49 (2013) 291–293.

10. R. A. Ambade, S. B. Ambade, R. R. Salunke, V. Malgras, S. H. Jin, Y. Yamauchi, S.-H Lee, Flexible-wire shaped all-solid-state supercapacitors based on facile electropolymerization of polythiophene with ultra-high energy density, J. Mater. Chem. A 4 (2016) 7406–7415.

11. Y. Shao, M. F. El-kady, L. J. Wang, Q. Zhang, Y. Li, H. Wang, M. F. Mousavi, R. B. Kaner, Graphene-based materials for flexible supercapacitors, Chem. Soc. Rev. 44 (2015) 3639–3665.

12. E. Armelin, M. M. Pérez-Madrigal, C. Alemán, D. Díaz Díaz, Current status and challenges of biohydrogels for applications as supercapacitors and secondary batteries, J. Mater. Chem. A 4 (2016) 1792–1805.

13. A. A. White, M. S. Platz, D. M. Aruguete, S. L. Jones, L. D. Madsen, R. D. Wesson, The National Science Foundation's investment in sustainable chemistry, engineering, and materials, ACS Sustainable Chem. Eng. 1 (2013) 871–877.

14. M. Pääkkö, J. Vapaavuori, R. Silvennoinen, H. Kosonen, M. Ankerfors, T. Lindström, L. A. Berglund, O. Ikkala, Long and entangled native cellulose I nanofibers allow flexible aerogels and hierarchically porous templates for functionalities, Soft Matter 4 (2008) 2492–2499.

15. L. Hu, G. Zheng, J. Yao, N. Liu, B. Weil, M. Eskilsson, E. Karabulut, Z. Ruan, S. Fan, J. T. Bloking, M. D. McGehee, L. Wågberg, Y. Cui, Transparent and conductive paper from nanocellulose fibers, Energy Environ. Sci. 6 (2013) 513–518.

16. L. Nyholm, G. Nyström, A. Mihranyan, M. Strømme, Toward flexible polymer and paper-based energy storage devices, Adv. Mater. 23 (2011) 3751–3769.

17. Y.-Z. Zhang, Y. Wang, T. Cheng, W. Y. Lai, H. Pang, W. Huang, Flexible supercapacitors based on paper substrates: A new paradigm for low-cost energy storage, Chem. Soc. Rev. 44 (2015) 5181–5199.

18. M. M. Pérez-Madrigal, M. G. Edo, C. Alemán, Powering the future: Application of cellulose-based materials for supercapacitors, Green Chem. 18 (2016) 5930–5956.

19. S. Dutta, J. Kim, Y. Ide, J. H. Kim, M. S. A. Hossain, Y. Bando, Y. Yamauchi, K. C. W. Wu, 3D network of cellulose-based energy storage devices and related emerging applications, Mater. Horizons 4 (2017) 522–545.

20. X. Du, Z. Zhang, W. Liu, Y. L. Deng, Nanocellulose-based conductive materials and their emerging applications in energy devices - A review, Nano Energy 35 (2017) 299–320.

21. W. S. Chen, H. P. Yu, S. Y. Lee, T. Wei, J. Li, Z. J. Fan, Nanocellulose: A promising nanomaterial for advanced electrochemical energy storage, Chem. Soc. Rev. 48 (2018) 2837–2872.

22. K. Gao, Z. Shao, J. Li, X. Wang, X. Peng, W. Wang, F. Wang, Cellulose nanofiber–graphene all solid-state flexible supercapacitors, J. Mater. Chem. A 1 (2013) 63–67.

23. K. Gao, Z. Shao, X. Wang, Y. Zhang, W. Wang, F. Wang, Cellulose nanofibers/multi-walled carbon nanotube nanohybrid aerogel for all-solid-state flexible supercapacitors, RSC Adv. 3 (2013) 15058–15064.

24. M. M. Pérez-Madrigal, M. G. Edo, M. G. Saborío, F. Estrany, C. Alemán, Pastes and hydrogels from carboxymethyl cellulose sodium salt as supporting

electrolyte of solid electrochemical supercapacitors, Carbohydr. Polym. 200 (2018) 456–467.

25. S. Kirchmeyer, R. Reuter, Scientific importance, properties and growing applications of poly(3,4-ethylenedioxythiophene), J. Mater. Chem. 15 (2005) 2077–3088.

26. C. R. G. Grenier, W. Pisula, T. J. Joncheray, K. Müllen, J. R. Reynolds, Regiosymmetric poly(dialkylphenylenedioxythiophene)s: Electron-rich, stackable π-conjugated nanoribbons, Angew. Chem. Int. Ed. 46 (2007) 714–717.

27. D. Mantione, I. del Agua, A. Sanchez-Sanchez, D. Mecerreyes, Poly(3,4-ethylenedioxythiophene) (PEDOT) derivatives: Innovative conductive polymers for bioelectronics, Polymers 9 (2017) 354.

28. L. J. del Valle, D. Aradilla, R. Oliver, F. Sepulcre, A. Gamez, E. Armelin, F. Estrany, C. Alemán, Cellular adhesion and proliferation on poly(3,4-ethylenedioxythiophene): Benefits in the electroactivity of the conducting polymer, Eur. Polym. J. 43 (2007) 2342–2349.

29. A. Guiseppi-Elie, Electroconductive hydrogels: Synthesis, characterization and biomedical applications, Biomaterials 31 (2010) 2701–2716.

30. M. C. G. Saborío, S. Lanzalaco, G. Fabregat, J. Puiggali, F. Estrany, C. Aleman, Flexible electrodes for supercapacitors based on the supramolecular assembly of biohydrogel and conducting polymer, *J. Phys. Chem. C* 122 (2018) 1078–1090.

31. C. Ocampo, R. Oliver, E. Armelin, C. Alemán, F. Estrany, Electrochemical synthesis of poly(3,4-ethylenedioxythiophene) on steel electrodes: Properties and characterization, J. Polym. Res. 13 (2006) 193–200.

32. M. C. G. Saborío, F. Estrany, C. Alemán, Properties of in situ polymerized poly(3,4-ethylenedioxythiophene)/alumina composites for energy storage applications, J. Polym. Sci. Part B: Polym. Phys. 55 (2017) 1131–1141.

33. W. J. Zheng, J. Gao, Z. Wei, J. Zhou, Y. M. Chen, Facile fabrication of self-healing carboxymethyl cellulose hydrogels, Eur. Polym. J. 72 (2015) 514–522.

34. G. Fabregat, J. Casanovas, E. Redondo, E. Armelin, C. Alemán, A rational design for the selective detection of dopamine using conducting polymers, Phys. Chem. Chem. Phys. 16 (2014) 7850–7861.

35. Y. Zhao, D.G. Truhlar, A new local density functional for main-group thermochemistry, transition metal bonding, thermochemical kinetics, and noncovalent interactions, J. Chem. Phys. 125 (2006) 194101.

36. S. F. Boys, F. Bernardi, The calculation of small molecular interactions by the differences of separate total energies. Some procedures with reduced errors, Mol. Phys. 19 (1970) 553–566.

37. D. Aradilla, F. Estrany, C. Alemán, Symmetric supercapacitors based on multilayers, J. Phys. Chem. C 115 (2011) 8430–8438.

38. F. Müller, C. A. Ferreira, D. S. Azambuja, C. Alemán, E. Armelin, Measuring the proton conductivity of ion-exchange membranes using electrochemical impedance spectroscopy and through-plane cell, *J. Phys. Chem. B* 118 (2014) 1102–1112.

39. Z. Niu, W. Zhou, J. Chen, G. Feng, H. Li, W. Ma, J. Li, H. Dong, Y. Ren, D. Zhao, S. Xie, Compact-designed supercapacitors using free-standing single-walled carbon nanotube films. Energy Environ. Sci. 4 (2011) 1440–1146.

40. M. Ujvári, M. Takács, S. Vesztergom, F. Bazsó, F. Ujhelyi, G. G. Láng, Monitoring of the electrochemical degradation of PEDOT films on gold using the bending beam method, J. Solid State Electrochem. 15 (2011) 2341–2349.

41. A. Puiggalí-Jou, M. M. Pérez-Madrigal, L. J. del Valle, E. Armelin, M. T. Casas, C. Michaux, E. A. Perpète, F. Estrany, C. Alemán, Confinement of a β-barrel protein in nanoperforated free-standing nanomembranes for ion transport. Nanoscale 8 (2016) 16922–16935.

42. H. Warrena, M. Panhuis Electrical conductivity and impedance behavior of hydrogels. Proc. of SPIE 9171 (2014) 3–8.

CAPTIONS TO FIGURES

Figure 1. Scheme illustrating the different synthetic steps used to produce [PEDOT/Al$_2$O$_3$/NaCMC]PHMeDOT electrodes: (a) preparation of PEDOT films by chronoamperometry and processing by mechanical stirring into MPs (a representative SEM micrograph of PEDOT MPs is displayed); (b) homogenization of Al$_2$O$_3$ particles by mechanical stirring (a representative SEM micrograph of Al$_2$O$_3$ particles is displayed); (c) formation of PEDOT/Al$_2$O$_3$/NaCMC using a 1.5 M citric acid aqueous solution for the cross-linking; and (d) *in situ* anodic polymerization of HMeDOT using PEDOT MPs are polymerization nuclei to produce [PEDOT/Al$_2$O$_3$/NaCMC]PHMeDOT.

Figure 2. Low and high magnification SEM micrographs (left and right, respectively) of the hydrogels used to prepare the electrodes: (a) PEDOT/Al$_2$O$_3$/NaCMC and (b) [PEDOT/Al$_2$O$_3$/NaCMC]PHMeDOT. Details of the surface and internal morphology of [PEDOT/Al$_2$O$_3$/NaCMC]PHMeDOT hydrogel: (c) PEDOT MP coated by PHMeDOT and (d-e) PHMeDOT sticks connecting PEDOT MPs at the (d) surface and (e) inside the hydrogel (cross section SEM image).

Figure 3. (a) FTIR and (b) Raman spectra (excitation wavelength: 785 nm) of NaCMC, PEDOT/Al$_2$O$_3$/NaCMC and [PEDOT/Al$_2$O$_3$/NaCMC]PHMeDOT. (c) Model compounds used to represent NaCMC: CMCn with n= 1, 2 or 3. Binding energies (BE, in kcal/mol) of neutral (*i.e.* CMC$n$$\cdots$2EDOT) and charged complexes (*i.e.* CMC$n$$\cdots$2EDOT^{+1}, CMC$n$$\cdots$Na$^+$ and ClO$_4^-$$\cdots$2EDOT^{+1}) calculated at the M06L/6-31G(d,p).

Figure 4. (a) Variation of the swelling ratio (SR) of NaCMC/NaCl and [PEDOT/Al$_2$O$_3$/NaCMC]PHMeDOT in 0.1 M NaHCO$_3$ and photographs before (left) and after (right) immersion in 0.1 M NaHCO$_3$ for 24 hours. (b) SEM micrographs of

NaCMC/NaCl hydrogel used as solid supporting electrolyte. (c) TGA and DTGA curves recorded for NaCMC/NaCl, PEDOT/Al$_2$O$_3$/NaCMC and [PEDOT/Al$_2$O$_3$/NaCMC]PHMeDOT hydrogels. TGA profiles were recorded at a heating rate of 10 ºC/min under controlled nitrogen atmosphere.

Figure 5. (a) Scheme of the assembled OESC prototype: C, A and SE refer to the cathode, anode and solid electrolytic medium, respectively. (b) Photograph of the steel ring used as mould for the fabrication of the hydrogels used as electrodes and the solid electrolyte. A photograph of the [PEDOT/Al$_2$O$_3$/NaCMC]PHMeDOT electrode is included. (c) Scheme of the assembled cellulose-based OESC prototype in the moulds and the press used for the assembly process. (d) Photographs of the assembly process and of the final cellulose-based OESC prototype. Photographs illustrating (e) the flexibility of the hydrogel used as solid electrolyte and (f) the compression reached by the OESC.

Figure 6. (a) Photograph of the supercapacitor prototype with the steel electrodes used for electrochemical characterization. (b) Cyclic voltammograms of the supercapacitor prototype recorded at 50 mV/s, varying the initial / final potential from – 0.50 V to 0.0 V while the reversal potential was kept fixed at 0.8 V. (c) Cyclic voltammograms of the supercapacitor prototype recorded at 50 and 100 mV/s scan rates. Initial and final potentials: -0.30 V; reversal potential: 0.8 V. (d) Variation of the specific capacitance (*SC*) against the number of oxidation-reduction cycles. (d-e) GCD cycles recorded at 0.00165 mA. The prototype was subjected to 2500 cycles (d). Magnification of the first and last ten cycles is displayed in (e).

Figure 7. (a) Nyquist (the inset corresponds to an amplified area from for better visualization of the low frequency zone) and (b, c) Bode plots of the NaCMC-based OESC. (d) Equivalent circuit model used to fit the experimental data.
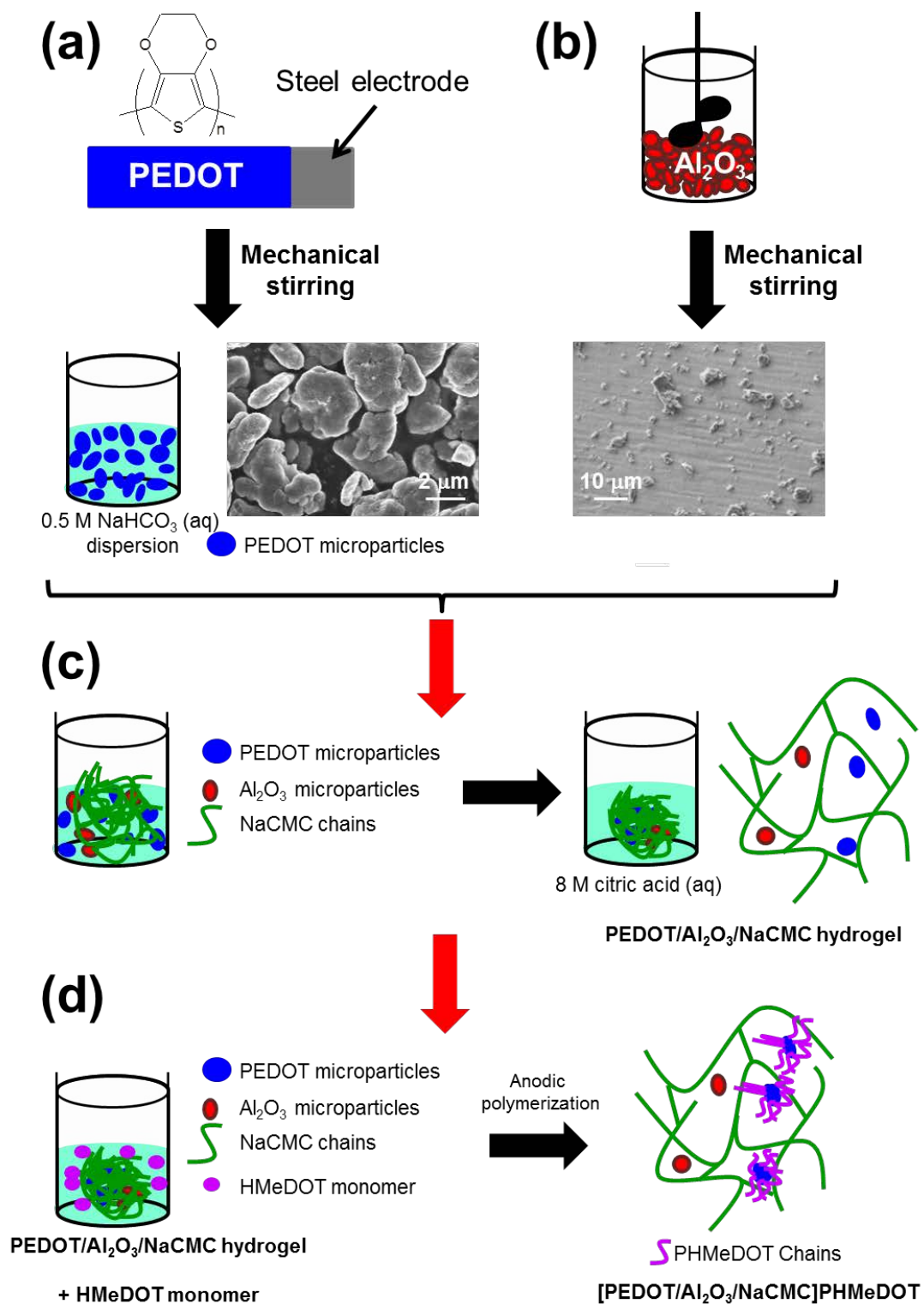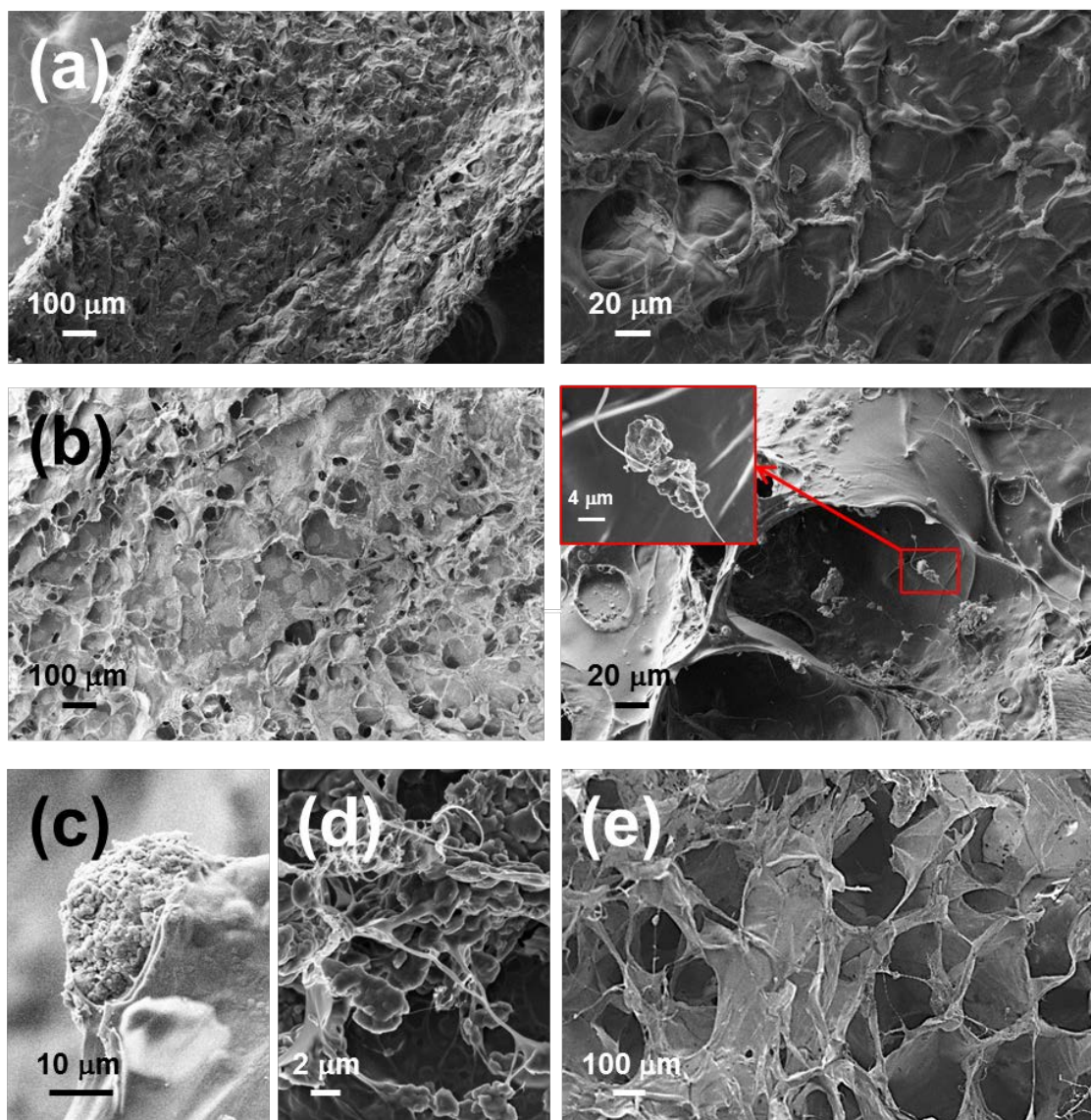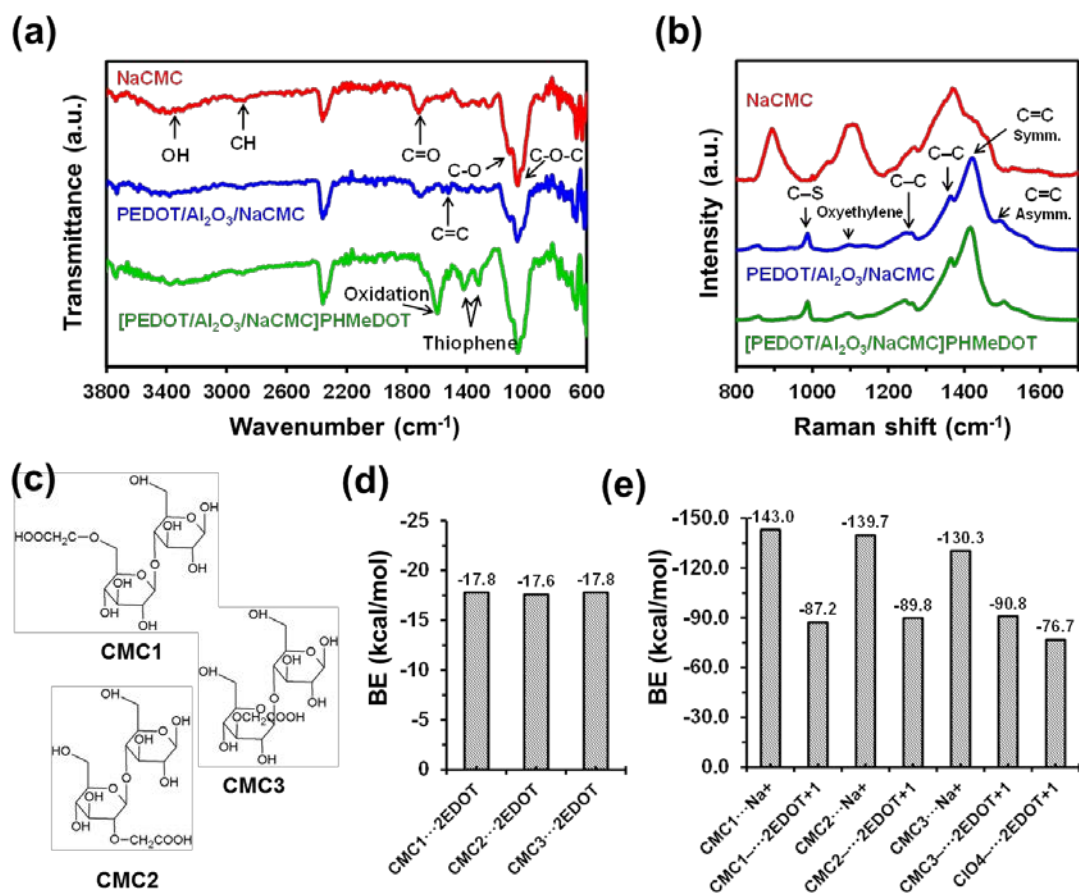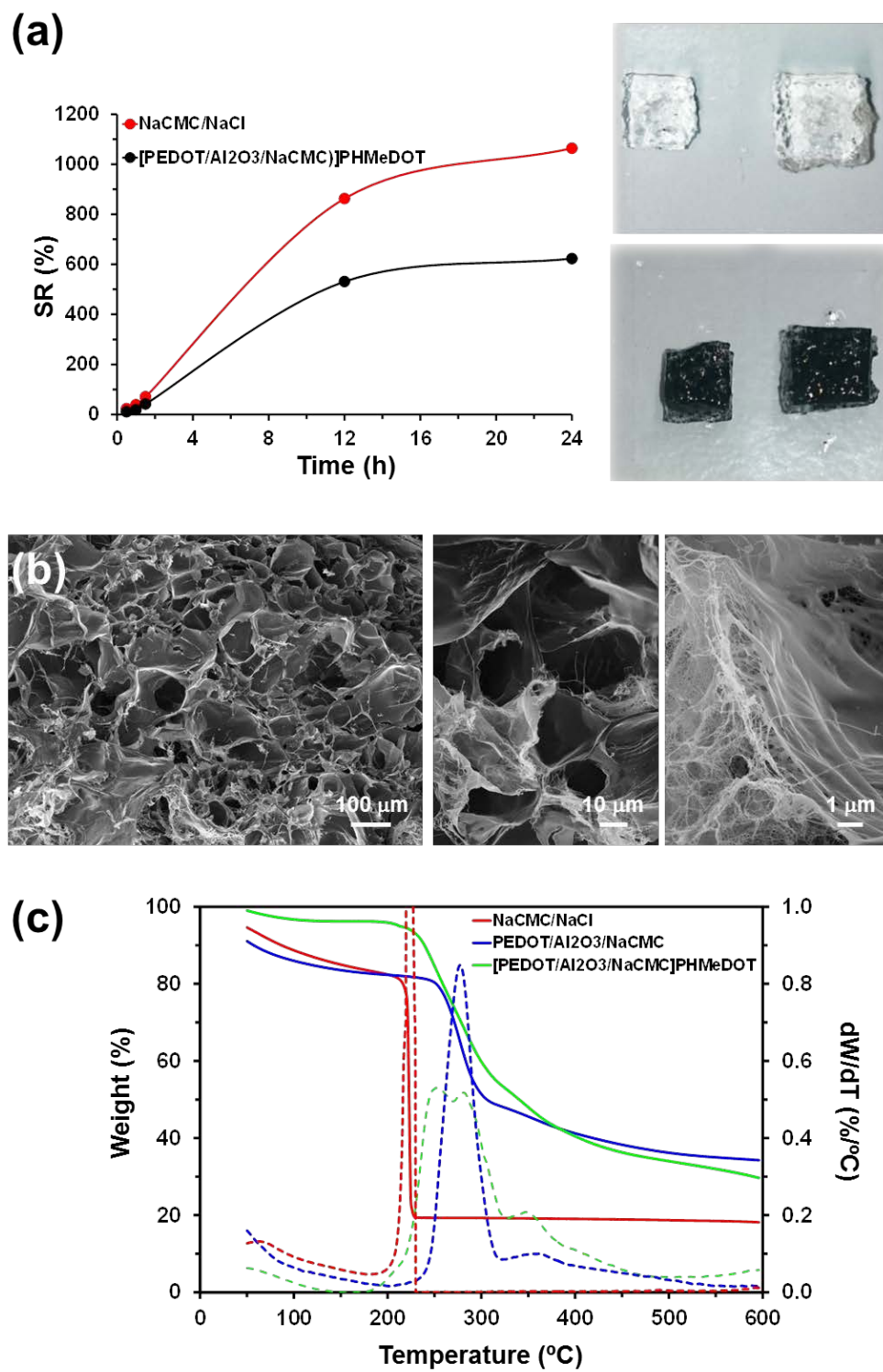
Figure 1

Figure 2

Figure 3

Figure 4

(a)

(b)

(c)

1.0 cm

0.35 cm

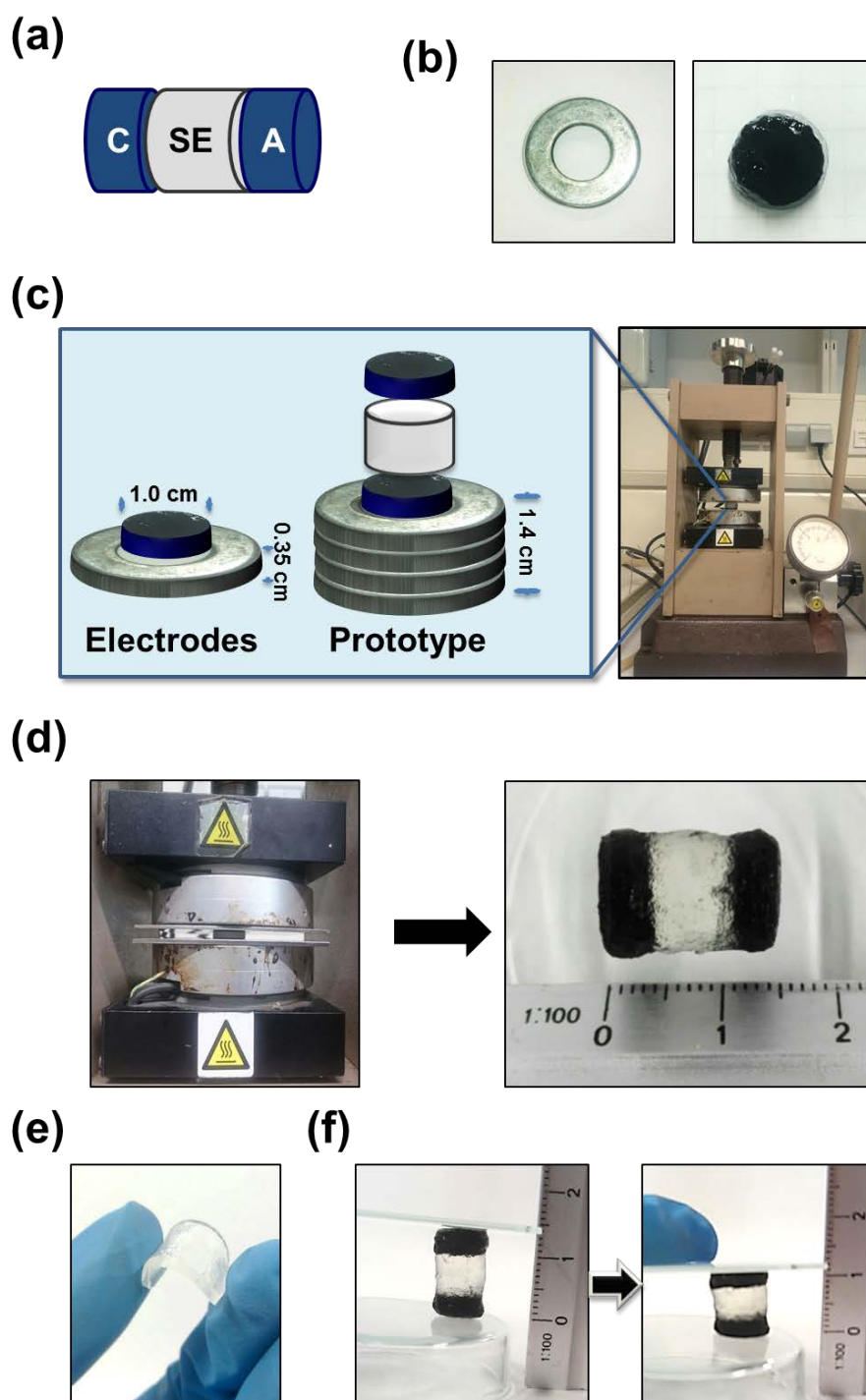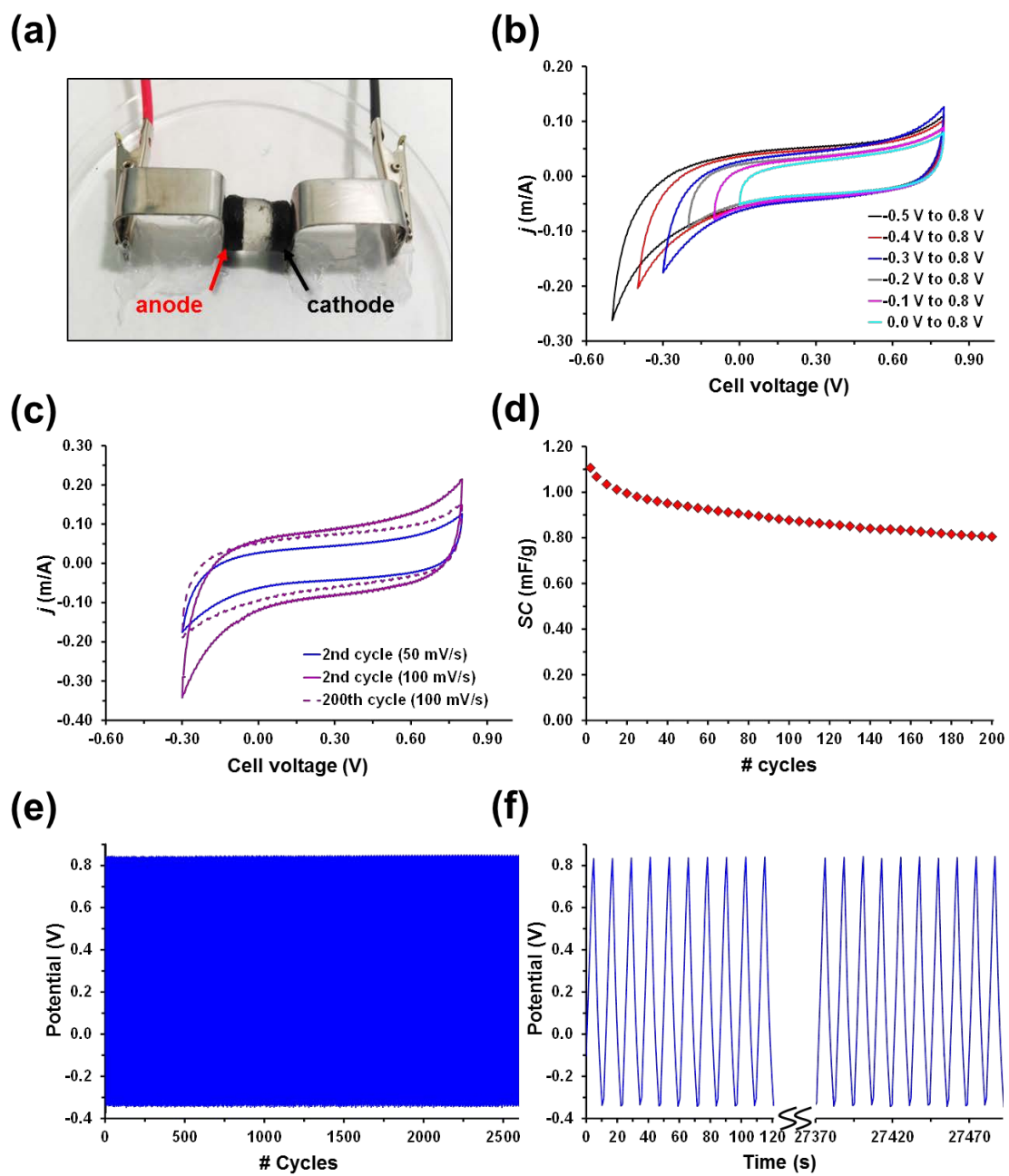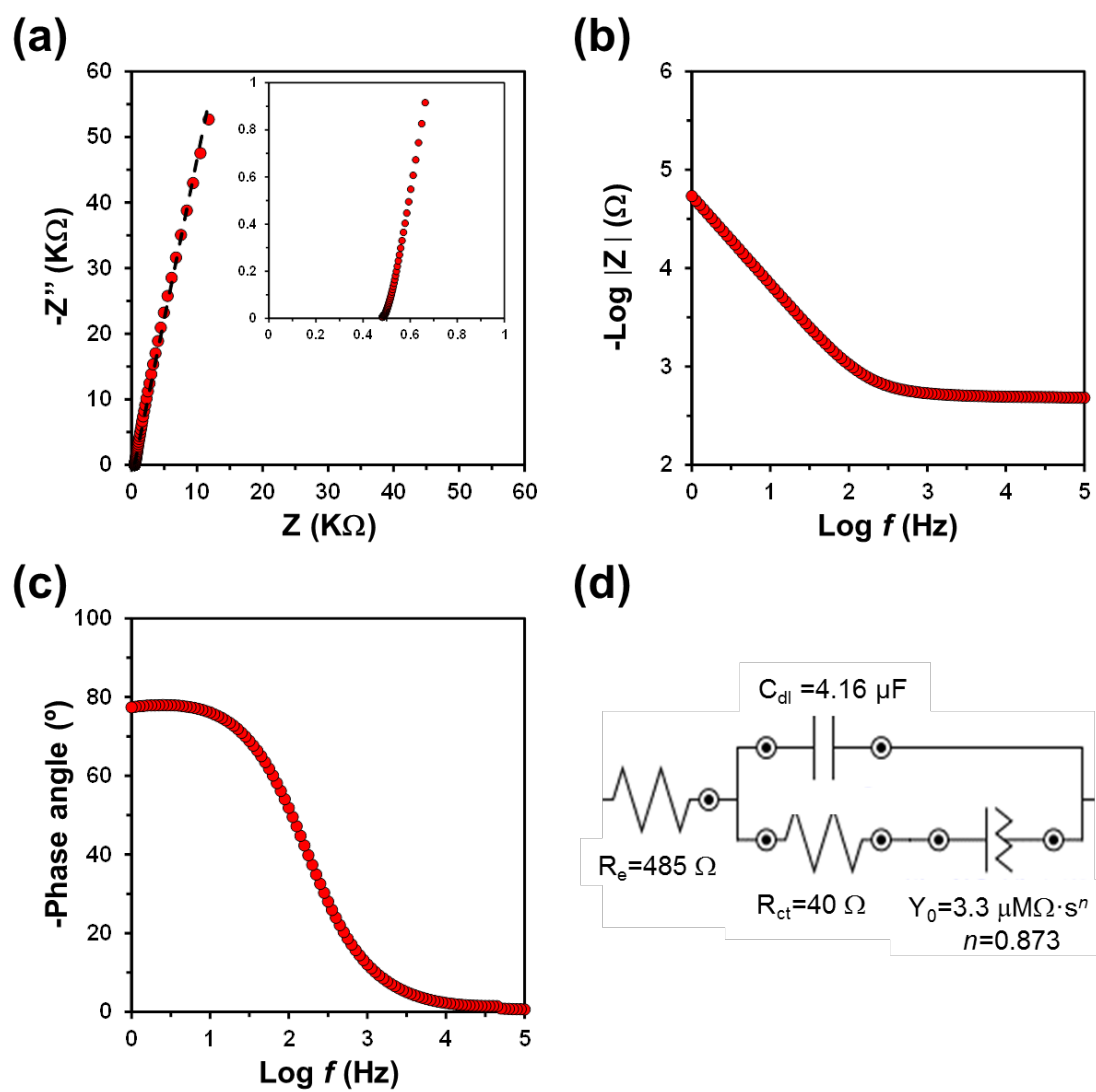1.4 cm

Electrodes   Prototype

(d)

(e)   **(f)**

Figure 5

Figure 6

Figure 7

GRAPHICAL ABSTRACT